

We are IntechOpen, the world's leading publisher of Open Access books Built by scientists, for scientists

5,800

Open access books available

142,000

International authors and editors

180M

Downloads

Our authors are among the

154

Countries delivered to

TOP 1%

most cited scientists

12.2%

Contributors from top 500 universities



WEB OF SCIENCE™

Selection of our books indexed in the Book Citation Index
in Web of Science™ Core Collection (BKCI)

Interested in publishing with us?
Contact book.department@intechopen.com

Numbers displayed above are based on latest data collected.
For more information visit www.intechopen.com



Chapter

Internal Microchannel Manufacturing Using Stereolithographic 3D Printing

Bastián Carnero, Carmen Bao-Varela, Ana Isabel Gómez-Varela and María Teresa Flores-Arias

Abstract

Internal channels are one of the most interesting structures to implement in microfluidics devices. Unfortunately, the optical technologies typically used in microfluidics, such as photolithography or reactive ion etching, are unable to generate these structures by only allowing surface structuring. Stereolithographic 3D printing has emerged as a very promising technology in internal microchannel manufacturing, by allowing a layer-by-layer structuring in volume performed by a laser that photopolymerises a liquid resin. Recent advances in laser technologies have reached resolutions of tens of micrometres. The high resolution of this type of printer, which a priori would allow the fabrication of channels of the same dimensions, may pose a problem by impeding the evacuation of uncured resin. In this chapter, the compromise between size and resin evacuation will be evaluated to find the optimal diameter range in which unobstructed and accurate microchannels can be obtained.

Keywords: stereolithography, 3D printing, microchannel, microfluidics, laser

1. Introduction

The 3-dimensional (3D) printing has recently become one of the most promising and ground-breaking manufacturing techniques [1–3], allowing to produce highly detailed structures, following simple and systematic steps without the need of the very expensive equipment of traditional technologies that normally require the use of cleaning rooms in large facilities. The 3D printing has facilitated the access to complex processes of manufacturing to a lot of researchers and many and varied industries [4]. Among others, the microfluidics field is a clear beneficiary from the role that 3D printing plays in the microfabrication processes [5], where techniques such as reactive ion etching (RIE) [6] and photolithography [7, 8] that produce a significant polluting chemical waste are predominant.

In addition to its multiple applications in chemistry, engineering or sensing, microfluidics is of great interest in medicine and pharmacology, where one of the challenges is to manufacture complex devices capable of mimicking physiological structures [9–11], such as vessels, veins and arteries, where novel drugs can be tested

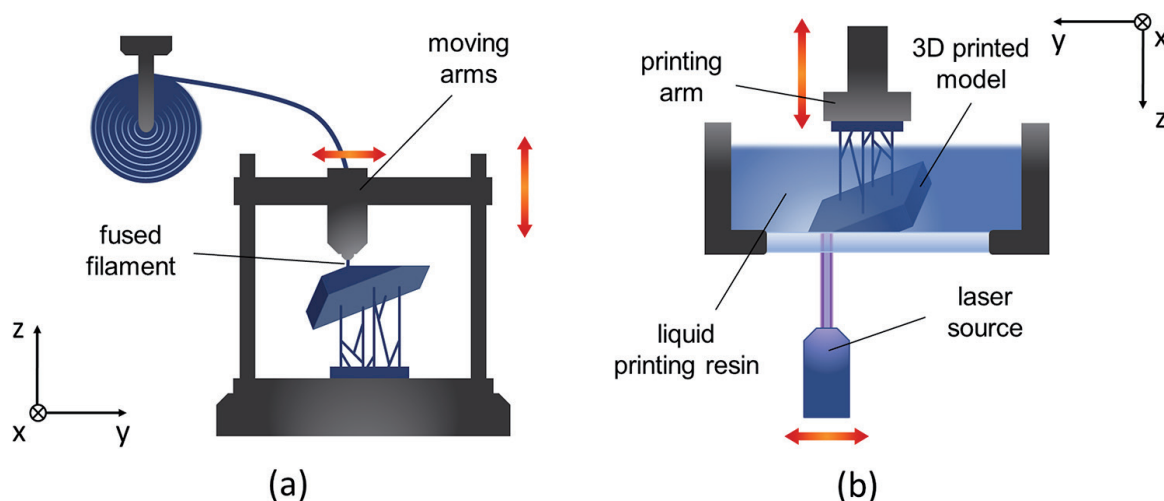


Figure 1. Popular 3D printing technologies: (a) fused deposition modelling (FDM) and (b) stereolithography (SLA).

under static and flow conditions (dynamic regime). These studies, much closer to reality than the studies carried out by traditional methods, involving testing in wells (static regime), could decrease the animal experimentation needed for testing drugs before the patient dispensation. All these devices are made up of different kinds of microchannels, capable of guiding small amounts of liquid samples. To be able to fabricate these devices, new technologies are required to manufacture them in a repeatable and accurate way. The 3D technology emerges as a promising one, since, it allows to achieve in an easy and fast way, microchannels with very high resolutions with simple procedures; to select different geometries for the microchannel profile (circular, rectangular, triangular...) and to create channels on complex surfaces in 3D or even internally.

Currently, two 3D printing technologies stand out above the rest [12, 13]: fused deposition modelling (FDM) [14, 15] and stereolithography (SLA) [16, 17]. FDM printers are based on the extrusion of a heated polymeric filament fused, that forms consecutive layers of a piece (**Figure 1a**). SLA printers use photopolymerisation to selectively cure a liquid resin contained in a tank (**Figure 1b**), manufacturing the model in a precise layer by layer process.

Both technologies are widely used given their versatility and efficiency, but SLA offers the highest accuracies [18]. Given the high quality of the surfaces fabricated by SLA printers, a variety of biocompatible materials suitable for its use with this equipment have emerged, increasing the potential biological applications to be used for [19–22]. There are many examples that show the perspective of SLA printers for complex microfluidic devices fabrication regarding biological applications, thus, making them an option to be used by researchers focused on 3D printing of reliable accurate and biologically solvent microfluidic devices. However, some technical aspects must be considered to optimise the printing results.

1.1 Theoretical fundamentals of stereolithography

The polymerisation of photosensitive resins is mainly governed by two parameters [23]: penetration depth of the curing light and the minimum energy required for polymerisation. The penetration of light follows the well-known Beer-Lambert law of exponential light absorption given by:

$$P_z = P_0 e^{-z/D_p} \quad (1)$$

being P_z the light power measured at a depth z from the surface; P_0 , the power at the surface; and D_p , the depth reached when light intensity decreases by a factor $1/e$ of the surface intensity. Note that D_p is a factor that depends on the resin composition, which determines its absorbance characteristics (dispersion and absorption) [24]. Power terms can be rewritten in terms of energy (so z will become the cure depth when the appropriate amount of light is provided) to obtain the working curve equation for SLA 3D printers:

$$C_D = D_p \ln \left[\frac{E_0}{E_c} \right] \quad (2)$$

where C_D is the depth/thickness at which the light energy is sufficient to convert the liquid resin into a gel; E_0 is the energy of light at the surface; and E_c is the critical energy necessary to initiate photopolymerisation. According to the Beer-Lambert law, the exposed light intensity reaches its maximum value (E_{MAX}) at the surface of the resin, and decreases exponentially as light penetrates through the resin due to the attenuation of the absorbing medium.

In the resin, the photopolymerised volume increases with the ultraviolet (UV) irradiation until the resin reaches to the gel point, where it transforms from liquid to solid-state. D_p and E_c are parameters that depend on the chemical characteristics of the resins and can be determined by drawing a semi-log plot of C_D vs. E_0 obtaining a straight-line curve with slope D_p and an x-intercept of E_c [25]. Once D_p and E_c are known, it is possible to optimise printing process choosing properly the exposure parameters and achieving the designed piece properties. This is the key for obtaining good results with a high-resolution SLA printing, where minimising the thickness of the deposited and light cured layer to achieve the maximum detail is critical.

In most SLA printers, the light source used to perform photopolymerisation is a laser, so the XY resolution is given by the size of the laser spot on the surface. Knowing the aforementioned parameters, the user or printer manufacturer can choose the proper parameters of light exposure (scan speed, power) to optimise the curing conditions and achieve the best resolution for the final device. Another determining factor is the minimum Z-step allowed by the printing arm, which gradually raises the piece from the bottom of the tank, that determines the corresponding layer thickness for each resin (see **Table 1**).

Printing resin	Clear	Model	Tough	Amber	Flexible	Elastic	Dental
Z-step (μm)	25	25	50	50	50	100	100
Washing time (min.)	15 + 5	10	10 + 10	20	10 + 10	10 + 10	20
Biocompatibility	✓	×	×	✓	×	×	✓
Curing temperatures (°C)	60	60	70	70	60	60	80
Curing time (min.)	30	60	60	30	60	20	20
Transparency	✓	×	×	✓	✓	✓	✓

Table 1.
 Manufacturer characteristics of the resins used in this chapter.

Finally, one of the most important aspects to be analysed for obtaining suitable internal channels is the orientation of the designed device, thus, a deep study of the influence of the inclination of the device to be fabricated in the process of photopolymerisation is necessary in order to determine the configurations that provide better results. We have to realise that the printer will slice the piece in a series of layers parallel to the base so that if the original configuration is rotated, these layers will change together with the areas that will be cured. Hence, objects with high surface detail should be printed with an orientation that helps the accurate curing of the layers. It also happens in the case of internal channels, where a proper angle could favour the full evacuation of the wastes of liquid resin from its interior, avoiding clogging.

In this work, a study of the performance of an SLA 3D printer in microfluidic devices is presented. For this purpose, an annular piece with a series of internal channels of different diameters and angles will be designed and manufactured. The dependence on the printing orientation of the device in the results will be evaluated. The study will be made for seven different commercial printing resins.

2. Materials and methods

2.1 3D printing

A Form 3B printer (Formlabs, Somerville, Massachusetts) is used to print the devices to be studied. This printer features a new technology called Low Force Stereolithography, a step further in SLA printers designed to reduce the manufacturing stress that pieces undergo during printing. In brief, this technology combines a galvanometric system with a series of mirrors to grant an incidence of the laser beam ($\lambda = 405 \text{ nm}$, $P = 250 \text{ mW}$) perpendicular to the resin tank, whose base will be made of a flexible material capable of deforming when the piece is pushed on it. In this way, the accuracy of the 3D printed structures is improved, as a much more uniform deposition of the laser energy is ensured.

It is well known that the printing orientation will determine the features of the printed devices. Typically, suppliers recommend using 45° as printing orientation in order to optimise the process. Although this recommendation is useful for superficial structures, we realise that for internal channels, the evacuation of uncured resin can produce obstructed lumens [19]. To test the influence of the printing angle on the ability to create internal channels with good quality, a quarter annulus piece was designed (**Figure 2a**) containing seven internal channels oriented at 0° , 15° , 30° , 45° , 60° , 75° and 90° and printed (**Figure 2b**). This study was performed four times for each resin selected, varying the diameter of the internal channels each time. These pieces can be identified in **Figure 2a** as A, B, C and D, corresponding to microchannels with diameter of 250, 500, 1000 and 1500 μm , respectively.

2.2 Data acquisition

The measurement of the diameter was performed using a Nikon MM 400 metallurgic microscope (Nikon Instruments Europe B.V., Amsterdam, The Netherlands), that performs measurements in real time (**Figure 3a**), and an analysis NIS-Elements Nikon software (Nikon Instruments, Melville, USA), by adjusting a measurement circumference (**Figure 3b**) that the software allows to move and modify over the image. The channels were illuminated in transmission light configuration that allowed us to

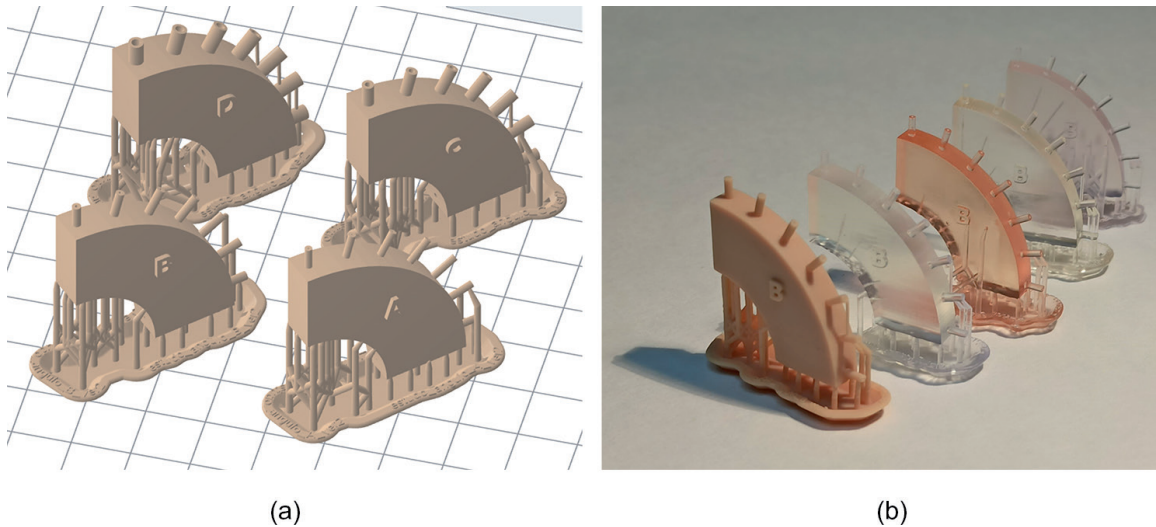


Figure 2. Picture of some 3D pieces: (a) image of the design used to study the formation of internal channel when varying printing angles and internal diameters, (b) picture of selected annulus printed for different resins, with theoretical internal diameters of $500\ \mu\text{m}$. From the fore to the ground: Model, Clear, Amber, Dental and Flexible resin. Scaffolding supporting the structures is shown.

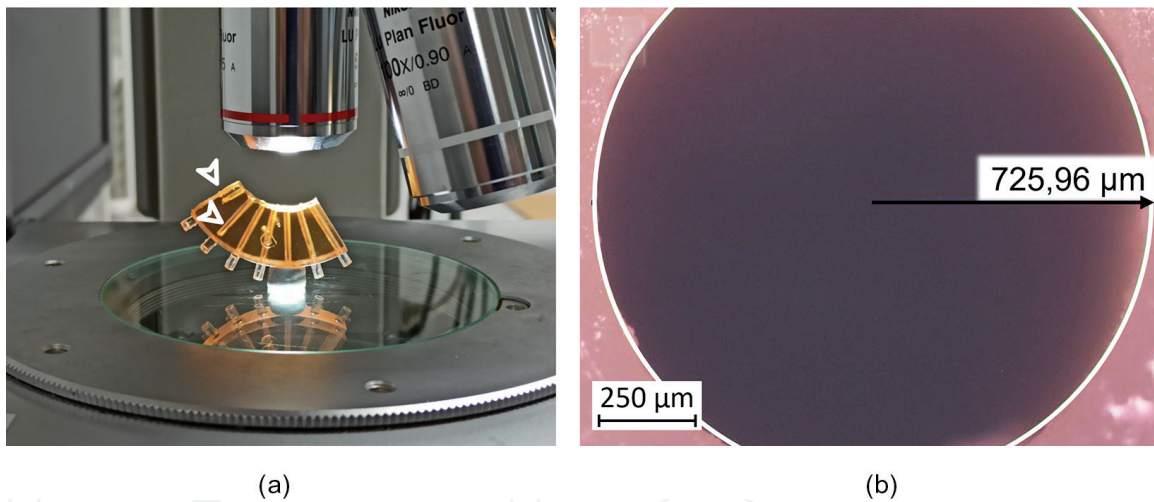


Figure 3. (a) Experimental configuration used to measure the internal channels of the quarter annulus using a microscope. White arrows point channels not fully formed, printed at 0° and 15° . (b) Microscope image of the end of a channel printed using Model resin, at an angle of 75° and a theoretical diameter of $1000\ \mu\text{m}$. The picture was taken with a $5\times$ microscope objective.

measure the lumen of each one. Images were acquired using a LU Plan Fluor objective (Nikon Instruments, Melville, USA) with $5\times$ magnification and a CCD camera Nikon DS-FI2 (Nikon Instruments, Melville, USA). Five measures were performed for each channel, obtaining a geometric mean and a standard deviation that will be presented in Section 3. Images of longitudinal sections of the microchannel internal surfaces were obtained with a 3D optical profilometer S neox (Sensofar Metrology, Terrassa, Spain) working in confocal mode.

2.3 Materials

Seven printing resins made by Formlabs for the Form 3B printer were studied: Dental LT V1, BioMed Amber V1, Elastic 50A V1, Clear V4, Model V2, Tough 2000 V1

and Flexible 80A V1. As introduced in Section 1.1, one of the critical factors to obtain high accuracy results with SLA printers is the Z-step of the printing arm allowed by every resin. Thus, the minimum Z-step was selected for each of them, as indicated in **Table 1**. Some of the used resins are even biocompatible (**Table 1**), which increases their potential applications.

After printing, it is necessary to post cure the resin pieces in a two-step process, to improve their mechanical aspects and superficial finishing. This process starts with a wash of the part in isopropanol >90% in the Form Wash tank (Formlabs, Somerville, Massachusetts), in one (Model, Amber and Dental) or two cycles (Clear, Tough, Flexible and Elastic), during times indicated in **Table 1**. The pieces are then left to dry and placed in the UV Form Cure chamber (Formlabs, Somerville, Massachusetts), which allows to control the temperature and is also provided with LEDs emitting at 405 nm. Curing temperatures and curing times can be consulted in **Table 1**.

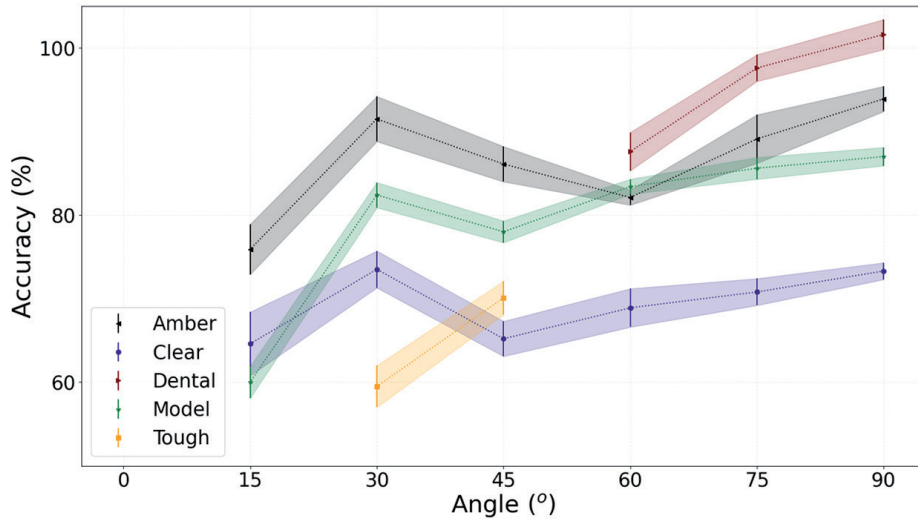
3. Results and discussion

The manufacturing of internal channels with a continuous and unobstructed lumen is one of the main challenges for actual SLA printers, because of their many applications in microfluidics [16, 17]. The fabrication of cavities in a bulk with a proper lumen is a very difficult process, since the photopolymerisation of each layer is sustained by the previous one, so the evacuation of the non-polymerised resin can be tedious.

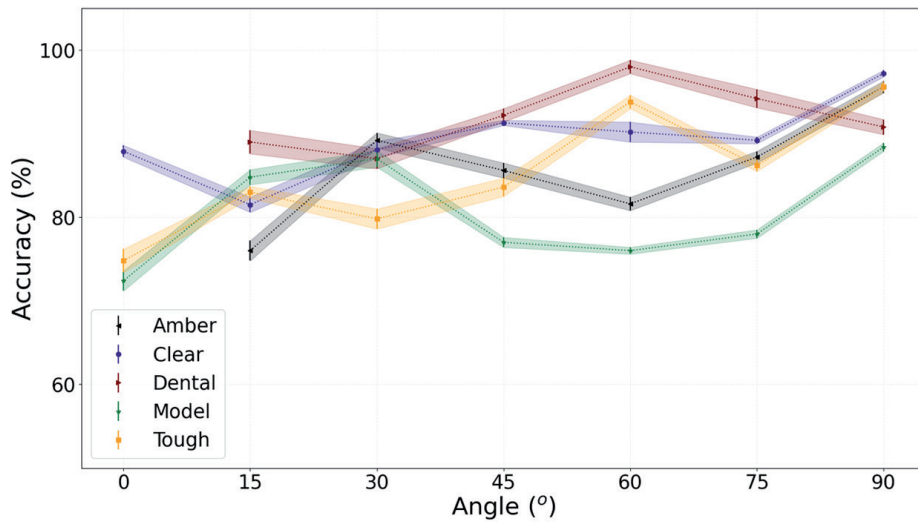
In many cases, the goal of obtaining unobstructed channels goes against the need for the printer to introduce scaffolds in the largest cavities, causing that internal channel collapse if some supports are not used during the printing. In addition, the own resolution of the printer can act as a limiter for very small channels, which do not have a structural challenge. In order to properly establish the dimensional limit between small channels and large cavities and to study the dependence of the internal channel performance on the diameter and angle of the printer, quarter annulus crossed by internal channels (**Figure 2**) were printed for each resin and the experimental diameters were measured as indicated in Section 2.2.

From the obtained results, three printing regimes can be defined. In the case of channels with small diameters (250 μm), no channel was fabricated for any resin at any angle, so no data can be presented. It can be concluded that, for these sizes, the formation of internal cavities in this range is not possible due to its small size, which prevents the correct evacuation of the resin. This implies that, the resolution for structures inside the printed piece is lower than the resolution for external ones, as structures of this size could be formed if they were made on the surface [19].

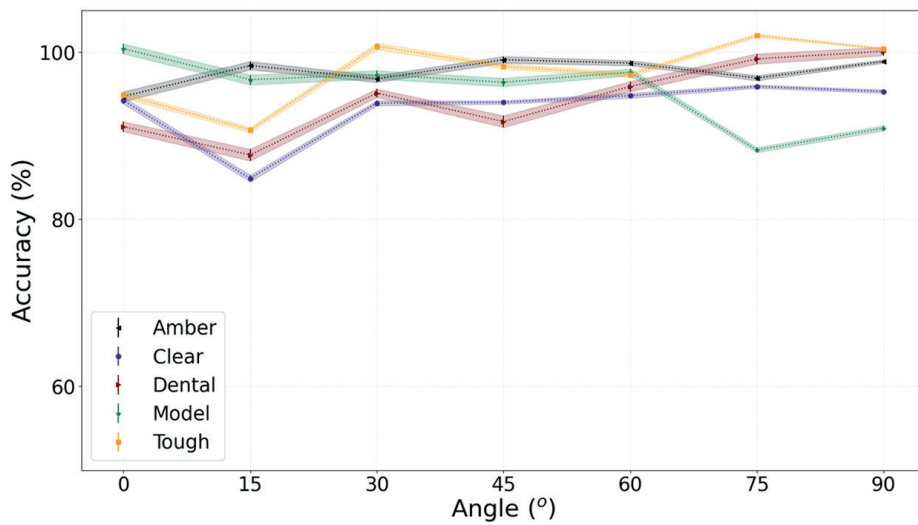
Next, for 500–1000 μm in diameter (medium diameters), channels begin to be formed (see **Figure 4a** and **b**) as will be detailed below. The bottom of these channels has been measured using the experimental configuration presented in **Figure 3**. We defined the accuracy as the ratio between the printed and theoretical designed diameter, in percentage. The tendency observed is an increase of experimental diameters as the printing angle increases, for a theoretical fixed value. For channels of 500 μm in diameter (**Figure 4a**), Amber and Dental resins provide the best results, almost reaching a 100% accuracy for an angle of 90°. In addition, for angles greater than 60°, they are all above 80% accuracy, together with Model resin. For lower values of the angles, the channels are narrower than those designed and are more incomplete (longitudinally) as the angle decreases, so for 15°, only Amber



(a)



(b)



(c)

Figure 4. Accuracy of the printing for the internal channels with diameters of (a) 500 μm , (b) 1000 μm and (c) 1500 μm in diameter, respectively. The error bars represent the standard deviation of the accuracies, and the area between the errors has been filled to facilitate the interpretation of the graphs.

Clear and Model resins form channels and for 0° , none. Longitudinally, Clear and Dental only form complete channels for 90° while Amber resin enables the formation of complete channels for 60° , 75° and 90° . For other values, the channels are not completely formed, although the unobstructed length of the channel increases as the angle increases (see **Figure 3a**).

When channels of $1000\ \mu\text{m}$ in diameter (**Figure 4b**) are fabricated, the printing accuracy suffers a global increase, being always above 70% for every studied angle. As the angle increase, an improvement in the precision is observed, and from 45° , all resins show an accuracy of more than 80% (except for Model, which shows a more irregular trend). The best results are obtained for 90° , where all the resins are above 90%, being the Model resin the exception, reaching an 88%.

In the case of channels with $1500\ \mu\text{m}$ in diameter (wide channels), an 85% on accuracy is achieved for all channels at every studied angle (**Figure 4c**). The length of the channels increases until they form completely (unobstructed) at 45° for Clear resin and at 15° for Amber and Dental resin. For greater angles, complete channels are formed for these resins. For these diameters, results are particularly suitable for angles greater than 60° degrees, where all resins show a printing accuracy greater than 95%, being the exception again the accuracy of Model resin, which is much closer to 90%. Therefore, internal channel with wide diameters allows to fabricate internal cavities for any angle and do not need scaffolding inside. Note that, in the case of the Tough and Model resin, the length of the channels cannot be evaluated by naked eye due to their opacity.

Channels fabricated at 45° and $500\ \mu\text{m}$ in diameter were chosen for inspecting the internal surface of unobstructed channels. In particular, Tough, Clear and Model resins were selected to be analysed because of their different properties (Z-step, biocompatibility, transparency...). **Figure 5** shows confocal images of longitudinal sections of the channels, where it can be observed that semi-circular designed profile is properly translated to the printed pieces.

By comparing the confocal images of the Tough (**Figure 5a**) vs. Clear and Model resins (**Figure 5b** and **c**), a decrease of the surface waviness with the Z-step is observed. The smoothest profile was achieved using the Model resin (**Figure 5c**).

From the previous analysis, we realise that the angle of impression is critical and has a major influence in preventing (**Figure 6a**) or favouring (**Figure 6b**) the formation of internal channels, so a larger angle (closer to 90°) is observed as the most suitable for channels to form properly and to have dimensions closer to those designed. The other key parameter found in this study is the diameter. As we have seen, a larger diameter allows results to be obtained with a higher resolution.

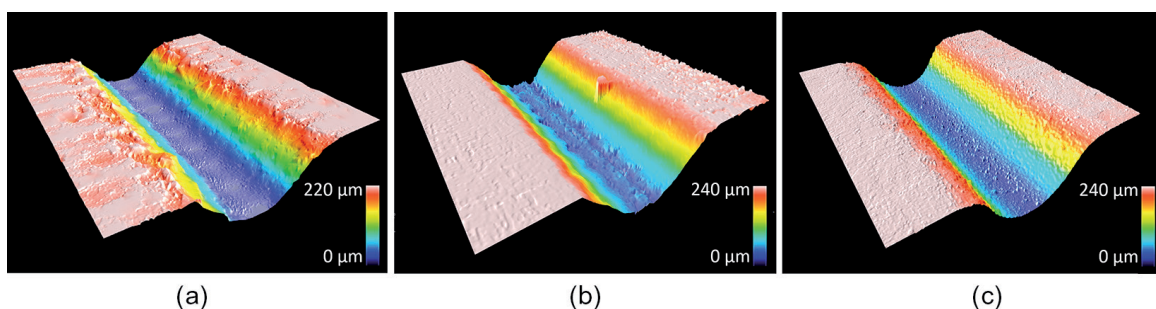


Figure 5. Confocal images of sections of channels designed with $500\ \mu\text{m}$ in diameter and printed at 45° using: (a) Tough, (b) Clear and (c) Model resin.

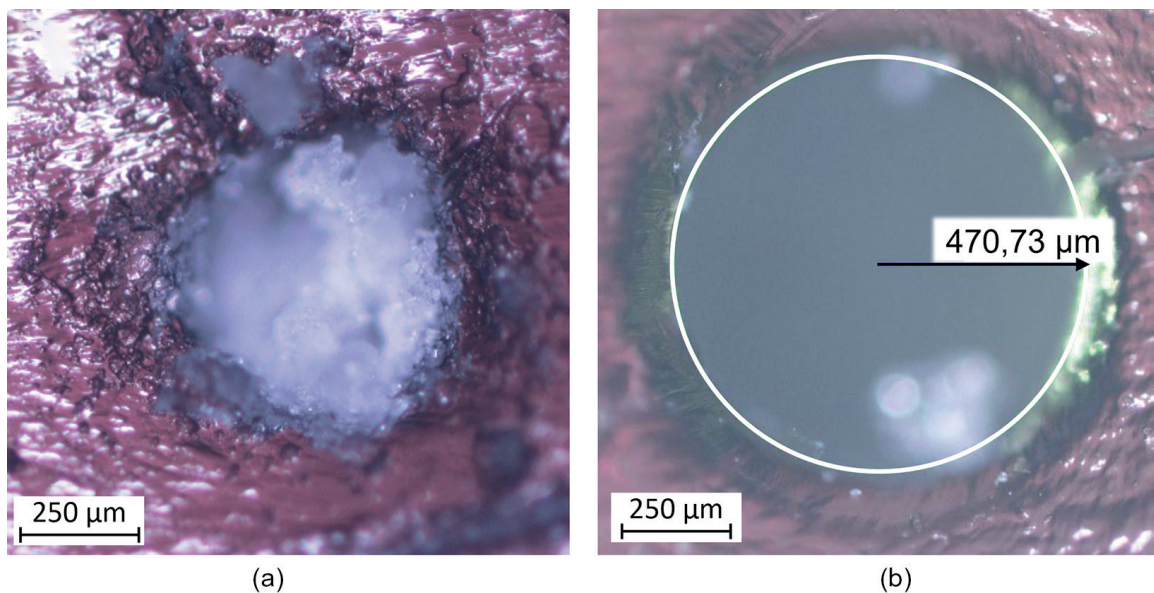


Figure 6. Microscope images of (a) obstructed and (b) unobstructed channels, with 500 μm of theoretical diameter, printed with amber resin at 0° and 75° , respectively. The images were taken with a 5X microscope objective.

The fact that orientation and diameter are so critical in the manufacture of channels is rooted in the way SLA printers operate and is intimately related to the evacuation of uncured resin, which will be more likely to occur the larger the channel and the more perpendicular the channel to the base (so gravity can enhance evacuation).

4. Conclusions

Microfluidics is a multidisciplinary field that needs versatile technologies capable for manufacturing structures with high accuracy in a precise and reliable way. 3D printing seems to be a promising technology to researchers and industries through easy procedures and a low pollution process. In particular, stereolithographic 3D printers become very attractive due to the developments achieved in lasers, making them one of the most promising choices with greater accuracy and finishing within the existing manufacturing technologies.

The performance in internal channel manufacturing of an SLA 3D printer is tested, since this is one very important piece in several microfluidic devices. Several resins (Clear, Dental, Tough, Amber, Flexible, Elastic and Model) was used for printing the internal channels in terms of accuracy (from hundreds to thousands of micrometres). For this, an annular piece containing several internal channels with different diameters and at different angles was designed and printed for each resin, to analyse the achievable range of dimensions and accuracy.

In light of the results, resin accumulation was found to be the key element behind the correct formation of the channels. This has its origin in the operation principle of SLA printers, based on the layer by layer photopolymerisation of a liquid resin contained in a tank. Thus, the uncured resin must be properly evacuated from the successive layers if a suitable cavity without obstructions and malformations wants to be obtained. It was found that there are two critical parameters: the diameter of the channels and the printing orientation of the device.

While no channel formation was observed for diameters of 250 μm for any of the fabrication angles neither the studied resins, from 500 μm onwards, open lumens

began to form. This was the case of Dental and Amber resin, which form channels with printing accuracy (ratio between the printed and theoretical designed diameter) over 80% for values of the angles above 60° and diameters above 500 µm.

In the case of larger diameters (around 1000 µm), the measured accuracies were greater than 70% for every studied resin and grew with the angle. For channels with a diameter of 1500 µm, it was found that all the resins achieved higher accuracy than 90%, so this range can be considered the optimum for the manufacture of complete and fully functional internal channels.

In conclusion, SLA 3D printers are one of the promising technologies in the fabrication of internal channels, showing interesting and promising results for channels of hundreds of micrometres in dimension, very suitable for the growing field of microfluidics. However, the formation of complete internal channels is difficult below 250 µm due to the incomplete evacuation of the uncured resin. There is still room for improvement, and it will be necessary to find both light sources and printing resins that allow higher accuracies, of the order of several tens of micrometres.

Acknowledgements

This work has been sponsored by contracts AEI RTI2018-097063-B-100, AEI/FEDER, UE; ED431B 2020/29; ED431E 2018/08 and ED481D-2021-019, Consellería de Cultura, Educación y Universidade Xunta de Galicia/FEDER e Estructuración Xunta de Galicia, IN607A2019-02. B. Carnero thanks to GAIN/Xunta de Galicia by the contract under no. 11_IN606D_2021_2604925.

Conflict of interest

The authors declare that they have no known competing financial interests or personal relationships that could have appeared to influence the work reported in this chapter.

IntechOpen

IntechOpen

Author details


Bastián Carnero^{1,2}, Carmen Bao-Varela¹, Ana Isabel Gómez-Varela¹
and María Teresa Flores-Arias^{1*}

1 Photonics4Life Research Group, Applied Physics Department, Instituto de
Materiais (iMATUS), Campus Vida, Universidade de Santiago de Compostela,
Santiago de Compostela, Spain

2 BFlow S.L., Edificio Emprendia, Santiago de Compostela, Spain

*Address all correspondence to: maite.flores@usc.es

IntechOpen

© 2022 The Author(s). Licensee IntechOpen. This chapter is distributed under the terms of the Creative Commons Attribution License (<http://creativecommons.org/licenses/by/3.0>), which permits unrestricted use, distribution, and reproduction in any medium, provided the original work is properly cited. 

References

- [1] Jones N. Science in three dimensions: The print revolution. *Nature*. 2012; **487**(7405):22-23
- [2] Bozkurt Y, Karayel E. 3D printing technology; methods, biomedical applications, future opportunities and trends. *Journal of Materials Research and Technology*. 2021;**14**:1430-1450. DOI: 10.1016/j.jmrt.2021.07.050
- [3] Palmara G, Frascella F, Roppolo I, Chiappone A, Chiadò A. Functional 3D printing: Approaches and bioapplications. *Biosensors & Bioelectronics*. 2021;**175**:112849
- [4] Sandeep B, Kannan TTM, Chandradass J, Ganesan M, John Rajan A. Scope of 3D printing in manufacturing industries—A review. *Materials Today: Proceedings*. 2021;**45**:6941-6945. DOI: 10.1016/j.matpr.2021.01.394
- [5] Bhattacharjee N, Urrios A, Kang S, Folch A. The upcoming 3D-printing revolution in microfluidics. *Lab on a Chip*. 2016;**16**(10):1720-1742
- [6] Nabesawa H, Hitobo T, Wakabayashi S, Aasji T, Abe T, Seki M. Polymer surface morphology control by reactive ion etching for microfluidic devices. *Sensors and Actuators B: Chemical*. 2008;**132**(2):637-643
- [7] Liu RH, Stremmer MA, Sharp KV, Olsen MG, Santiago JG, Adrian RJ, et al. Passive mixing in a three-dimensional serpentine microchannel. *Journal of Microelectromechanical Systems*. 2000;**9**(2):190-197
- [8] Lohse M, Heinrich M, Grützner S, Haase A, Ramos I, Salado C, et al. Versatile fabrication method for multiscale hierarchical structured polymer masters using a combination of photo- and nanoimprint lithography. *Micro and Nano Engineering*. 2021; **10**:100079. DOI: 10.1016/j.mne.2020.100079
- [9] Casas-Arozamena C, Otero-Cacho A, Carnero B, Almenglo C, Aymerich M, Alonso-Alconada L, et al. Haemodynamic-dependent arrest of circulating tumour cells at large blood vessel bifurcations as new model for metastasis. *Scientific Reports*. 2021;**11**(1):23231
- [10] Aymerich M, Álvarez E, Bao-Varela C, Moscoso I, González-Juanatey JR, Flores-Arias MT. Laser technique for the fabrication of blood vessels-like models for preclinical studies of pathologies under flow conditions. *Biofabrication*. 2017;**9**(2):025033. DOI: 10.1088/1758-5090/aa6c3d
- [11] Chen YY, Kingston BR, Chan WCW. Transcribing in vivo blood vessel networks into in vitro perfusable microfluidic devices. *Advanced Materials Technologies*. 2020;**5**:2000103. DOI: 10.1002/admt.202000103
- [12] Rupal BS, Garcia EA, Ayranci C, Qureshi AJ. 3D printed 3D-microfluidics: Recent developments and design challenges. *Journal of Integrated Design and Process Science*. 2019;**22**(1):5-20. DOI: 10.3233/jid-2018-0001
- [13] Zhu F, Macdonald NP, Cooper JM, Wlodkovic D. Additive manufacturing of lab-on-a-chip devices: Promises and challenges. *Micro/Nano Materials, Devices, and Systems*. 2013;**8923**:892344
- [14] Romanov V, Samuel R, Chaharlang M, Jafek AR, Frost A, Gale BK. FDM 3D printing of

- high-pressure, heat-resistant, transparent microfluidic devices. *Analytical Chemistry*. 2018;**90**(17):10450-10456. DOI: 10.1021/acs.analchem.8b02356
- [15] Cailleaux S, Sanchez-Ballester NM, Gueche YA, Bataille B, Soulairol I. Fused deposition modeling (FDM), the new asset for the production of tailored medicines. *Journal of Controlled Release*. 2021;**330**:821-841. DOI: 10.1016/j.jconrel.2020.10.056
- [16] Heidt B, Rogosic R, Bonni S, Passariello-Jansen J, Dimech D, Lowdon JW, et al. The liberalization of microfluidics: Form 2 benchtop 3D printing as an affordable alternative to established manufacturing methods. *Physica Status Solidi*. 2020;**217**:1900935. DOI: 10.1002/pssa.201900935
- [17] Moreno-Rivas O, Hernández-Velázquez D, Piazza V, Marquez S. Rapid prototyping of microfluidic devices by SL 3D printing and their biocompatibility study for cell culturing. *Materials Today: Proceedings*. 2019;**13**:436-445. DOI: 10.1016/j.matpr.2019.03.189
- [18] Gong H, Bickham BP, Woolley AT, Nordin GP. Custom 3D printer and resin for 18 μm \times 20 μm microfluidic flow channels. *Lab on a Chip*. 2017;**17**(17):2899-2909
- [19] Carnero B, Bao-Varela C, Gómez-Varela AI, Álvarez E, Flores-Arias MT. Microfluidic devices manufacturing with a stereolithographic printer for biological applications. *Materials Science and Engineering: C*. 2021;**129**:112388
- [20] Krefß S, Schaller-Ammann R, Feiel J, Priedl J, Kasper C, Egger D. 3D printing of cell culture devices: Assessment and prevention of the cytotoxicity of photopolymers for stereolithography. *Materials (Basel)*. 2020;**13**(13):3011
- [21] Hart C, Didier CM, Sommerhage F, Rajaraman S. Biocompatibility of blank, post-processed and coated 3D printed resin structures with electrogenic cells. *Biosensors*. 2020;**10**(11):152
- [22] Xu X, Goyanes A, Trenfield SJ, Diaz-Gomez L, Alvarez-Lorenzo C, Gaisford S, et al. Stereolithography (SLA) 3D printing of a bladder device for intravesical drug delivery. *Materials Science and Engineering: C*. 2021;**120**:111773. DOI: 10.1016/j.msec.2020.111773
- [23] Jacobs PF. *Fundamentals of Stereolithography*. Valencia, California: Society of Manufacturing Engineers; 1992. pp. 196-211
- [24] Lee JH, Prud'homme RK, Aksay IA. Cure depth in photopolymerization: Experiments and theory. *Journal of Materials Research*. 2001;**16**(12):3536-3544. DOI: 10.1557/JMR.2001.0485
- [25] Bennett J. Measuring UV curing parameters of commercial photopolymers used in additive manufacturing. *Additive Manufacturing*. 2017;**18**:203-212